Modeling of a Single-chamber Microbial Fuel Cell Using Glycerin as an Energy Source

Bunpot Sirinutsomboon, Napatsanun Wongsamajan, Katanyuta Sirikhum

Thammasat University, Thailand

0342

The Asian Conference on Sustainability, Energy & the Environment 2013

Official Conference Proceedings 2013

Abstract

A bio-electrochemical system of microbial fuel cell (MFC) can operate on wastewater and various organic substances. One possible energy source is crude glycerin waste from biodiesel production. Similar to any process, MFC needs accurate computational models for prediction and optimization of the cell performance. We proposed a comprehensive computational modeling of a membrane-less single-chamber MFC, in which bacteria consumed glycerin as a primary nutrient. The simulated cathode was a layer of silicone, which prevented water leakage, but allowed oxygen molecules to diffuse through to take part in the reduction reaction. Bulk liquid in the chamber contained glycerin being consumed during the operation. Glycerin molecules diffused through the biofilm, which deposited on the anode surface, and were oxidized by the bacteria dispersive within the film. The biofilm was assumed to be conductive; therefore electrons generated from the oxidation reaction within the film could migrate toward the anode surface. We developed the simulation program to accept inputs such as initial amount of glycerin, thickness of the biofilm layer, and dimensions of the MFC chamber. Some outputs of the program include profiles of concentrations of glycerin and oxygen as a function of time and location, and the MFC output voltage as a function of time.

Keywords microbial fuel cell, single chamber, air cathode, glycerin, simulation

Introduction

A properly designed system of electrochemical cell can operate using a liquid culture of bacteria. Such system is called microbial fuel cell (MFC) (Logan et al., 2006). An MFC can treat wastewater containing organic matters, which bacteria can consume as a mean of wastewater treatment, while simultaneously producing electricity. Crude glycerin as a by-product of biodiesel production process has a potential to be used by an MFC without glycerin purification process (Feng et al., 2011). Utilization of crude glycerin by large-scale MFCs can synergistically boost the biodiesel production industry.

MFCs typically come with two chambers of anode and cathode, separated by a proton exchange membrane (PEM). Our interest is, however, a membrane-less single-chamber MFC (Liu and Logan, 2004). One side of a cathode electrode of the MFC is in contact with the liquid, while the other side is directly exposed to air. In this manner, oxygen in the air can passively diffuse through the cathode and involve in the reaction of oxygen reduction. An intensive energy task of liquid aeration is not required, thus saving cost and energy. A PEM can obstruct the flow of the protons from the anode chamber to the cathode. A study (Liu and Logan, 2004) showed that an air-cathode MFC produced higher power output in absence of the membrane. PEMs are also generally quite expensive; therefore we are interested in an MFC without a PEM. A membrane-less single-chamber MFC has a simple configuration and is inexpensive to build. Figure 1 shows a conceptual diagram of the MFC having glycerin ($C_3H_8O_3$) as a primary source of energy.

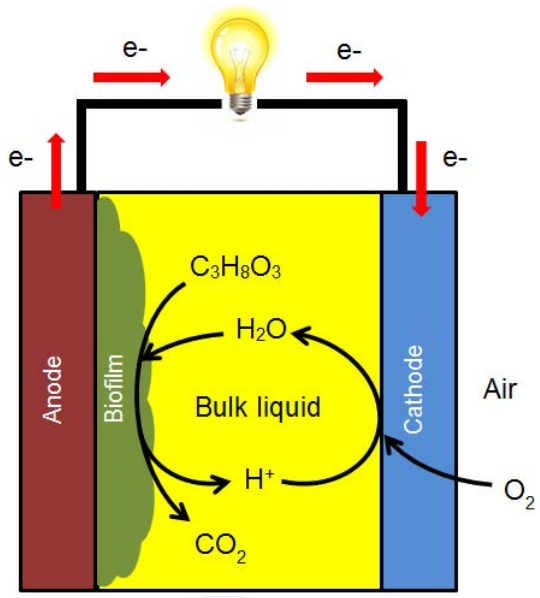

Figure 1. A conceptual diagram of membrane-less single-chamber MFC.

As in any simulation, the aim is to have a mathematical model that can predict the output and performance of the MFC for future modifications and optimization of the system. The model requires knowledge in electrochemistry, reaction kinetics, and mass balances. It also includes diffusion of oxygen across the cathode, and diffusion of chemical species across the diffusion layers and the biofilm that deposits on the anode. Some attempts have been done to develop simulation models of biofilm on anode (Merkey and Chopp, 2012) and two-chambered MFCs (Zeng et al., 2010). No work for a comprehensive simulation of single-chambered MFCs has been published. To develop a computational program for such simulation is our goal.

Methods

For our MFC, the cathodic reaction was the reduction of oxygen (Logan et al., 2006), as shown in Equation 1, and the anodic reaction was the oxidation of glycerin (Selembo et al., 2009), as shown in Equation 2. The two equations were considered when deriving the equations for the rates of consumption or production of the chemical species in our system.

$$O_2 + 4H^+ + 4e^- \rightarrow 2H_2O \quad (1)$$

$$C_3H_8O_3 + 3H_2O \rightarrow 3CO_2 + 14H^+ + 14e^- \quad (2)$$

Our program was roughly divided into two sequential segments; cathode and biofilm/anode. Each segment has a number of equations to be solved and their calculated outputs will be used by the subsequent segment. The program was developed using Visual Basic.

Cathode

The concentration of oxygen in the silicone layer, assumed to be the main component of the cathode, was calculated using Fick's second law of diffusion (Zielke, 2006), as shown in Equation 3. The concentration was a function of both time and location in the silicone layer.

$$\frac{\partial}{\partial t}[O_2]_{\text{cat}} = D_{O_2,\text{sil}} \frac{\partial^2}{\partial y^2}[O_2]_{\text{cat}} \quad (3)$$

where

$[O_2]_{\text{cat}}$ = concentration of oxygen in cathode, mmol dm^{-3}

$D_{O_2,\text{sil}}$ = diffusivity of oxygen in silicone, μm^2 min^{-1}

y = location in silicone, μm

The cathode voltage was then calculated using the cathodic reaction and the Nernst equation, as shown in Equation 4 (Logan et al., 2006). Only oxygen molecules that diffused through the silicone layer could be reduced to yield water molecules. The reaction was assumed to occur only at the cathode/liquid interface and oxygen was assumed to be ideal gas.

$$E_{\text{cat}} = E^o_{\text{cat}} - \frac{RT}{\gamma_{e^-/O_2} F} \ln\left(\frac{1}{(R\times 10^{-2})T[O_2]_{\text{cat/liq}}[H^+]^4_{\text{cat/liq}}}\right) \quad (4)$$

where

E_{cat} = cathode voltage, V

E^o_{cat} = standard cathode voltage, V

R = gas constant, J mol^{-1} K^{-1}

T = temperature, K

γ_{e^-/O_2} = electron equivalence of oxygen, mmol-electron mmol-oxygen^{-1}

F = Faraday's constant, C mol^{-1}

$[O_2]_{\text{cat/liq}}$ = concentration of oxygen at cathode/liquid interface, mol dm^{-3}

$[H^+]_{\text{cat/liq}}$ = concentration of hydrogen ion at cathode/liquid interface, mol dm^{-3}

It was proposed that the rate of oxygen reduction at the cathode follows the Monod equation and the Butler-Volmer equation (Torres et al., 2010; Zeng et al., 2010). We thus incorporated the two equations into Equation 5.

$$r_{O_2} = k_{O_2} \frac{[O_2]_{\text{cat/liq}}}{K_{O_2}+[O_2]_{\text{cat/liq}}} exp\left[-\alpha_{\text{cat}}\gamma_{e^-/O_2}\frac{F}{RT}(E_{\text{cat}} - E^o_{\text{cat}})\right] \quad (5)$$

where

r_{O_2} = rate of oxygen reduction per area, mmol dm^{-2} min^{-1}

k_{O_2} = rate constant of oxygen reduction per area, mmol dm^{-2} min^{-1}

$[O_2]_{\text{cat/liq}}$ = concentration of oxygen at cathode/liquid interface, mmol dm^{-3}

K_{O_2} = half velocity constant for oxygen, mmol dm^{-3}

α_{cat} = electron-transfer coefficient of cathode

Biofilm/Anode

Glycerin was assumed to be the main nutrient consumed by the bacteria, which resulted in the anodic reaction shown in Equation 2. Since the bacteria were localized and dispersed throughout the biofilm, assumed to conduct electrons, we considered the biofilm to be part of the anode (Kato Marcus et al., 2007; Merkey and Chopp, 2012; Torres et al., 2010). The rate of glycerin consumption was the same as the rate of exogenous respiration by the bacteria and it was described by the Nernst-Monod equation (Kato Marcus et al., 2007; Merkey and Chopp, 2012), as shown in Equation 6. The active biomass referred to the live bacteria.

$$r_{\text{exo}} = \frac{\rho_b \mu_b X_b}{Y_b \gamma_{\text{COD/gly}}} \cdot \frac{[Gly]_{\text{bio}}}{K_{Gly}+[Gly]_{\text{bio}}} \cdot \frac{1}{1+exp\left(-\frac{F}{RT}\eta\right)} \quad (6)$$

where

r_{exo} = rate of exogenous respiration in biofilm, mmol dm^{-3} min^{-1}

ρ_b = density of active biomass, mg-VS dm^{-3}

(VS = volatile solids, a measure of biomass)

μ_b = specific growth rate of active biomass, min^{-1}

X_b = volume fraction of active biomass (unitless) = $\frac{\text{volume of active biomass}}{\text{bulk volume}}$

Y_b = active biomass growth yield, mg-VS mg-COD^{-1}

$\gamma_{\text{COD}/Gly}$ = COD equivalence of glycerin, mg-COD mmol-glycerin^{-1}

$[Gly]_{\text{bio}}$ = concentration of glycerin in biofilm, mmol dm^{-3}

K_{Gly} = half velocity constant for glycerin, mmol dm^{-3}

η = $E_{\text{ano}} - E_{K_{\text{ano}}}$ = local potential in biofilm, V

E_{ano} = anode voltage, V

$E_{K_{\text{ano}}}$ = Half-max-rate anode voltage, V

In addition to the exogenous respiration, from which the bacteria obtained most energy from, the bacteria performed endogenous respiration by oxidizing their own cellular mass for additional energy. The rate of endogenous respiration was described by Equation 7 (Kato Marcus et al., 2007; Merkey and Chopp, 2012).

$$r_{\text{endo}} = b_{\text{endo}} \rho_b X_b \frac{1}{1+exp\left(-\frac{F}{RT}\eta\right)} \quad (7)$$

where

r_{endo} = rate of endogenous respiration in biofilm, mg-VS dm^{-3} min^{-1}

b_{endo} = endogenous decay coefficient of active biomass, min^{-1}

Based on the steady-state electron balance and Ohm's law, we calculated the local potential in the biofilm using Equation 8 (Kato Marcus et al., 2007; Merkey and Chopp, 2012).

$$\kappa_{\text{bio}} \frac{\partial^2}{\partial z^2}\eta - \frac{F}{\tau \upsilon}\left(\gamma_{e^-/Gly} r_{\text{exo}} + \gamma_{e^-/b} r_{\text{endo}}\right) = 0 \quad (8)$$

where

κ_{bio} = biofilm conductivity, mS μm^{-1}

z = location in biofilm, μm

τ = time conversion = 60 sec min^{-1}

υ = volume conversion = 10^{15} μm^3 dm^{-3}

$\gamma_{e^-/Gly}$ = electron equivalence of glycerin, mmol-electron mmol-glycerin^{-1}

$\gamma_{e^-/b}$ = electron equivalence of active biomass, mmol-electron mg-VS^{-1}

(assuming $C_5H_7O_2N$ for VS (Kato Marcus et al., 2007))

The anode voltage was calculated using the anodic reaction and the Nernst equation, as shown in Equation 9 (Logan et al., 2006). The voltage value was applied as a boundary condition for calculation of Equation 8. Carbon dioxide was assumed to be ideal gas.

$$E_{\text{ano}} = E^o_{\text{ano}} - \frac{RT}{\gamma_{e^-/Gly} F} \ln\left(\frac{[Gly]_{\text{ano/bio}}}{\left((R\times 10^{-2})T[CO_2]_{\text{ano/bio}}\right)^3 [H^+]^{14}_{\text{ano/bio}}}\right) \quad (9)$$

where

E^o_{ano} = standard anode voltage, V

$[Gly]_{\text{ano/bio}}$ = concentration of glycerin at anode/biofilm interface, mol dm^{-3}

$[CO_2]_{\text{ano/bio}}$ = concentration of carbon dioxide at anode/biofilm interface, mol dm^{-3}

$[H^+]_{\text{ano/bio}}$ = concentration of hydrogen ion at anode/biofilm interface, mol dm^{-3}

The open-circuit voltage of the MFC was determined using Equation 10 (Logan et al., 2006).

$$E_{\text{OCV}} = E_{\text{cat}} - E_{\text{ano}} \quad (10)$$

where

E_{OCV} = open-circuit voltage of MFC, V

In the biofilm, the concentration of glycerin was a function of both time and location. We derived a mass balance of glycerin in the biofilm, as shown in Equation 11, by considering both the anodic reaction and the diffusion of glycerin from the bulk liquid through the biofilm layer. In a similar fashion, we derived mass balances of hydrogen ion and carbon dioxide, as shown in Equations 12 and 13, respectively.

$$\frac{\partial}{\partial t}[Gly]_{\text{bio}} = D_{Gly,\text{bio}} \frac{\partial^2}{\partial z^2}[Gly]_{\text{bio}} - r_{\text{exo}} \quad (11)$$

where

$D_{Gly,\text{bio}}$ = diffusivity of glycerin in biofilm, μm^2 min^{-1}

$$\frac{\partial}{\partial t}[H^+]_{\text{bio}} = D_{H^+} \frac{\partial^2}{\partial z^2}[H^+]_{\text{bio}} + 14r_{\text{exo}} \quad (12)$$

where

$[H^+]_{\text{bio}}$ = concentration of hydrogen ion in biofilm, mmol dm^{-3}

D_{H^+} = diffusivity of hydrogen ion in water, μm^2 min^{-1}

$$\frac{\partial}{\partial t}[CO_2]_{\text{bio}} = D_{CO_2,\text{bio}} \frac{\partial^2}{\partial z^2}[CO_2]_{\text{bio}} + 3r_{\text{exo}} \quad (13)$$

where

$[CO_2]_{\text{bio}}$ = concentration of carbon dioxide in biofilm, mmol dm^{-3}

$D_{CO_2,\text{bio}}$ = diffusivity of carbon dioxide in biofilm, μm^2 min^{-1}

All the parameters applied in the above equations were obtained from various literatures. Some assumptions were made, since not all aspects of MFC have been thoroughly studied yet. Numerical values of the parameters are shown in Table 1.

Table 1. Parameters in the simulation of the MFC.

Symbol	Description	Value	Unit	Reference
α_{cat}	electron-transfer coefficient of cathode	0.084	unitless	calculated, [1]
$\gamma_{\text{COD}/Gly}$	COD equivalence of glycerin	112	mg-COD mmol-glycerin^{-1}	calculated
$\gamma_{e^-/b}$	electron equivalence of active biomass	0.177	mmol-electron mg-VS^{-1}	[2]
$\gamma_{e^-/Gly}$	electron equivalence of glycerin	14	mmol-electron mmol-glycerin^{-1}	calculated
γ_{e^-/O_2}	electron equivalence of oxygen	4	mmol-electron mmol-oxygen^{-1}	calculated
κ_{bio}	biofilm conductivity	5×10^{-5}	mS μm^{-1}	[3]
μ_b	specific growth rate of active biomass	4.792×10^{-4}	min^{-1}	[3]
ρ_b	density of active biomass	5×10^{4}	mg-VS dm^{-3}	[3]
b_{endo}	endogenous decay coefficient of active biomass	5.556×10^{-5}	min^{-1}	[3]
$D_{CO_2,\text{bio}}$	diffusivity of carbon dioxide in biofilm	6.91×10^{4}	μm^2 min^{-1}	[4]
$D_{Gly,\text{bio}}$	diffusivity of glycerin in biofilm	1.41×10^{4}	μm^2 min^{-1}	[4]
D_{H+}	diffusivity of hydrogen ion in water	5.58×10^{5}	μm^2 min^{-1}	[5]
$D_{O_2,\text{sil}}$	diffusivity of oxygen in silicone	9.6×10^{4}	μm^2 min^{-1}	[6]
E^o_{ano}	standard anode voltage	0.0126	V	calculated, [7]
E^o_{cat}	standard cathode voltage	1.229	V	[8]
$E_{K_{\text{ano}}}$	Half-max-rate anode voltage	-0.448	V	[3]
F	Faraday's constant	96,485	C mol^{-1}	[2]
k_{O_2}	rate constant of oxygen reduction per area	5.48×10^{-6}	mmol dm^{-2} min^{-1}	calculated, [1]
K_{Gly}	half velocity constant for glycerin	0.0536	mmol dm^{-3}	assumed same as acetate, [3]
K_{O_2}	half velocity constant for oxygen	4×10^{-3}	mmol dm^{-3}	[1]
R	gas constant	8.3145	J mol^{-1} K^{-1}	[2]
X_b	volume fraction of active biomass	0.5	unitless	assumed
Y_b	active biomass growth yield	0.049	mg-VS mg-COD^{-1}	[3]

References: [1] - Zeng et al. (2010), [2] - Kato Marcus et al. (2007), [3] - Merkey and Chopp (2012), [4] - Stewart (2003), [5] - Torres et al. (2008), [6] - Zhang and Cloud (2006), [7] - Thauer et al. (1977), and [8] - Logan et al. (2006).

Numerical approximation

Several equations above are differential equations, and finding the solutions normally involves a numerical approximation method. The selected numerical technique was the implicit finite difference method (Zielke, 2006). For instance, we transformed Equation 3 into the following equation.

$$\frac{[O_2]_{i,j}-[O_2]_{i,j-1}}{t_j-t_{j-1}} = D_{O_2,\text{sil}}\left\{\frac{[O_2]_{i+1,j}-2[O_2]_{i,j}+[O_2]_{i-1,j}}{(z_i-z_{i-1})^2}\right\} \quad (14)$$

where

i = index indicating location i

j = index indicating time j

We rewrote Equation 14 into an equation of vectors and matrices that contained the values of the concentration of oxygen at every location in the silicone layer. For example, if we partition the layer to consist of 4 locations inside, Equation 14 then becomes Equation 15. The subscript t indicates that all the concentrations in the vector are at time t.

$$\frac{1}{\Delta t}\left(\begin{bmatrix}[O_2]_1\\ [O_2]_2\\ [O_2]_3\\ [O_2]_4\end{bmatrix}_t - \begin{bmatrix}[O_2]_1\\ [O_2]_2\\ [O_2]_3\\ [O_2]_4\end{bmatrix}_{t-\Delta t}\right) = \frac{D_{O_2,\text{sil}}}{(\Delta z)^2}\left(\begin{bmatrix}-2 & 1 & 0 & 0\\ 1 & -2 & 1 & 0\\ 0 & 1 & -2 & 1\\ 0 & 0 & 1 & -2\end{bmatrix}\begin{bmatrix}[O_2]_1\\ [O_2]_2\\ [O_2]_3\\ [O_2]_4\end{bmatrix}_t - \begin{bmatrix}[O_2]_0\\ 0\\ 0\\ [O_2]_5\end{bmatrix}\right) \quad (15)$$

where

Δt = $t_j - t_{j-1}$ = time interval

Δz = $z_i - z_{i-1}$ = distance interval

We could also rewrite Equation 15 into an abbreviated form, as shown in Equation 16.

$$\frac{1}{\Delta t}\left(\underline{[O_2]}_t - \underline{[O_2]}_{t-\Delta t}\right) = \frac{D_{O_2,\text{sil}}}{(\Delta z)^2}\left(\mathbb{A}\underline{[O_2]}_t - \underline{a}\right) \quad (16)$$

We then rearranged Equation 16 into the form of $\mathbb{B}\underline{x} = \underline{b}$, as shown in Equation 17. Since the matrix $\mathbb{B}$ was a tridiagonal matrix, we applied an algorithm for solving a tridiagonal system by elimination (Conte and de Boor, 1980) to solve for the vector $\underline{x}$, which was $\underline{[O_2]}_t$ in our case.

$$\left(\mathbb{I} - \frac{\Delta t D_{O_2,\text{sil}}}{(\Delta z)^2}\mathbb{A}\right)\underline{[O_2]}_t = \underline{[O_2]}_{t-\Delta t} + \frac{\Delta t D_{O_2,\text{sil}}}{(\Delta z)^2}\underline{a} \quad (17)$$

where

$\mathbb{I}$ = identity matrix

Results and discussions

We developed a simulation program of the MFC with a user-friendly interface. The program accepted inputs including initial amount of glycerin, operation time, pH, temperature, and biofilm thickness. A program user can also modify values of some parameters, if more

accurate values are acquired. Figure 2 show some screen captures of the program. The program displayed the results in two formats; tables of data and plots. The results included various variables of the system, for example, concentration of oxygen in cathode layer, concentration of glycerin and pH in bulk liquid, concentration of glycerin in biofilm layer, cathode and anode voltages, and MFC open-circuit voltage.

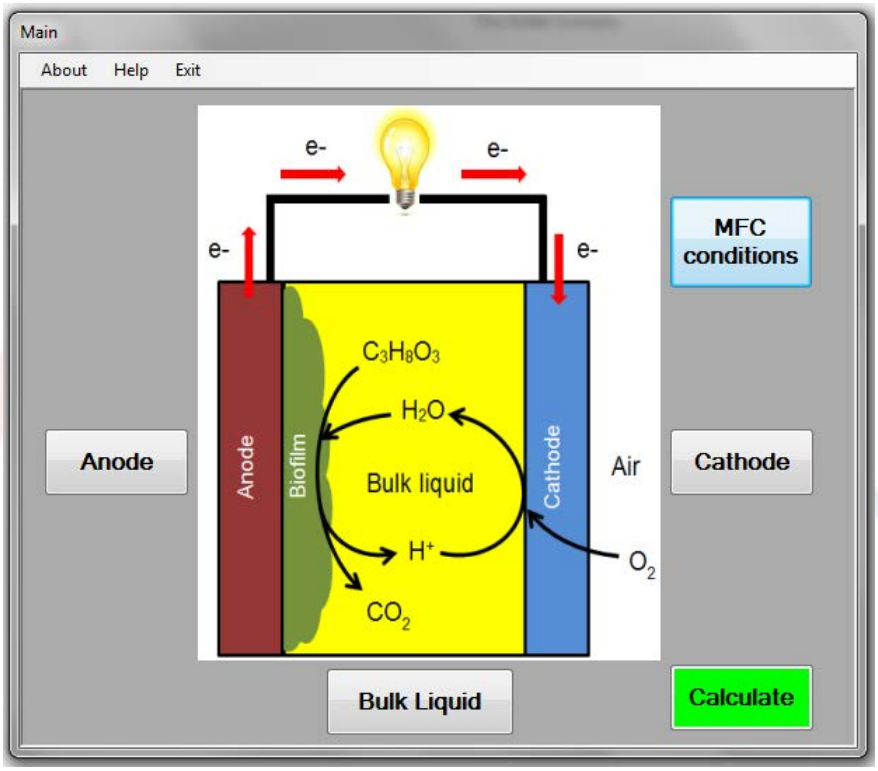

(A)

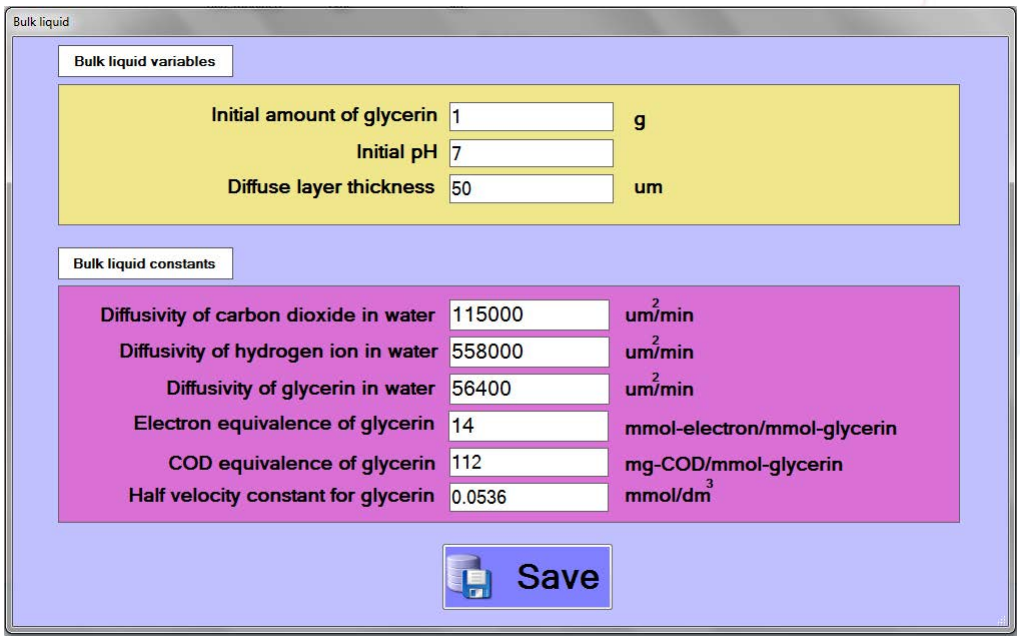

(B)

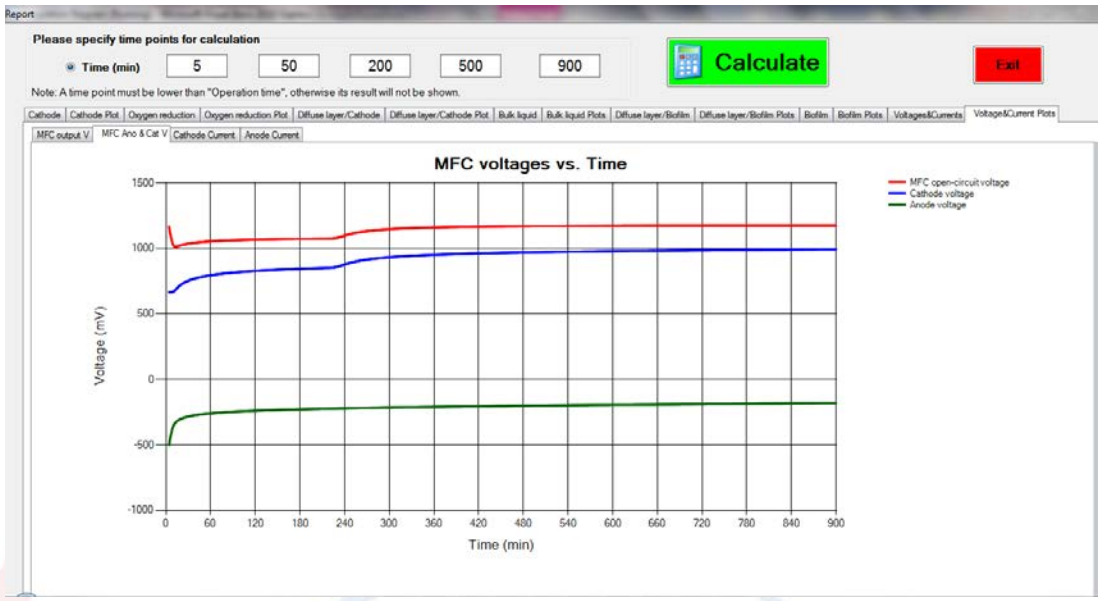

(C)

Figure 2. Examples of screen captures of the MFC simulation program: (A) the main window, (B) the input window of bulk liquid, and (C) the result window.

Plots of concentration of oxygen in the cathode layer at different times are shown in Figure 3. Thickness of the layer was set at 1000 μm. Oxygen concentration in the air was assumed to be in excess and thus constant. The liquid was depleted of oxygen since it was completely consumed in the reduction reaction. As shown in the plots, the concentration reached saturation in the first few minutes and remained constant throughout the MFC operation.

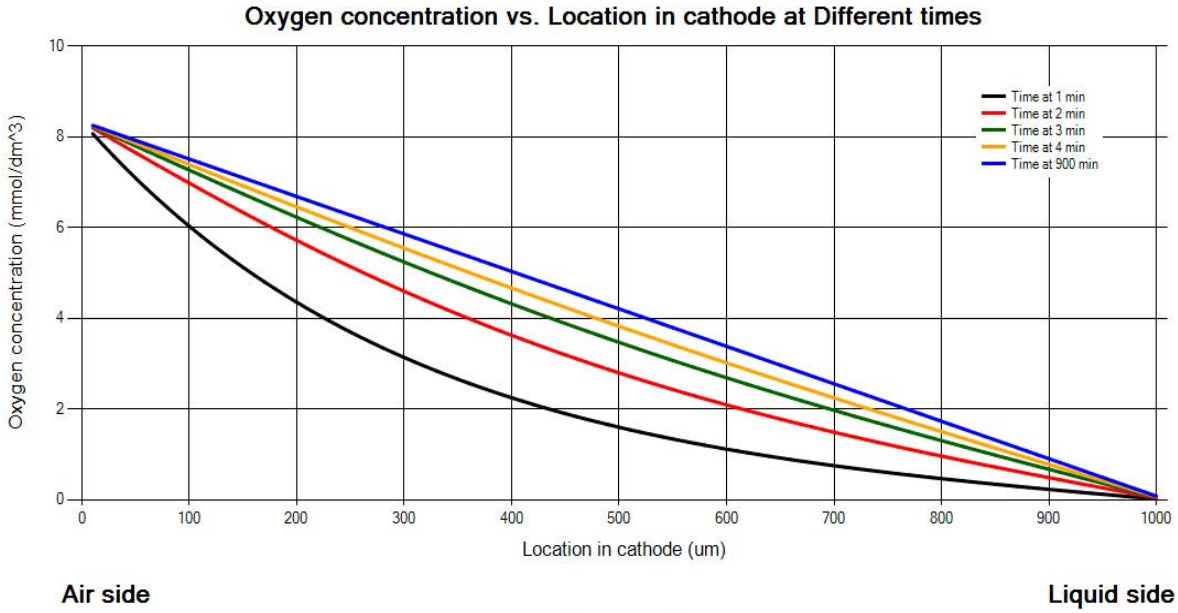

Figure 3. Plots of oxygen concentration in cathode layer at different times.

Plots of glycerin concentration and pH in the bulk liquid are shown in Figures 4 and 5, respectively. The MFC operation time was set at 15 hours (900 min). The glycerin concentration decreased, due to being consumed by the bacteria, quickly in the first hour and at a slower rate afterwards. The pH also decreased due to the accumulation of hydrogen ions, and thus the system became more acidic.

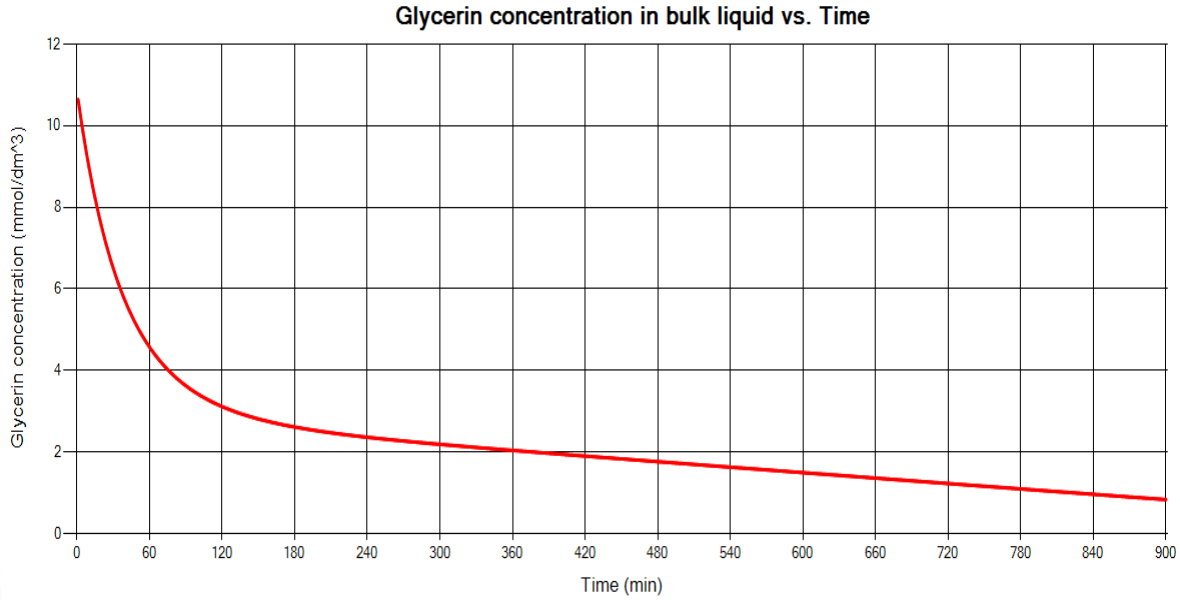

Figure 4. A plot of glycerin concentration in bulk liquid over time.

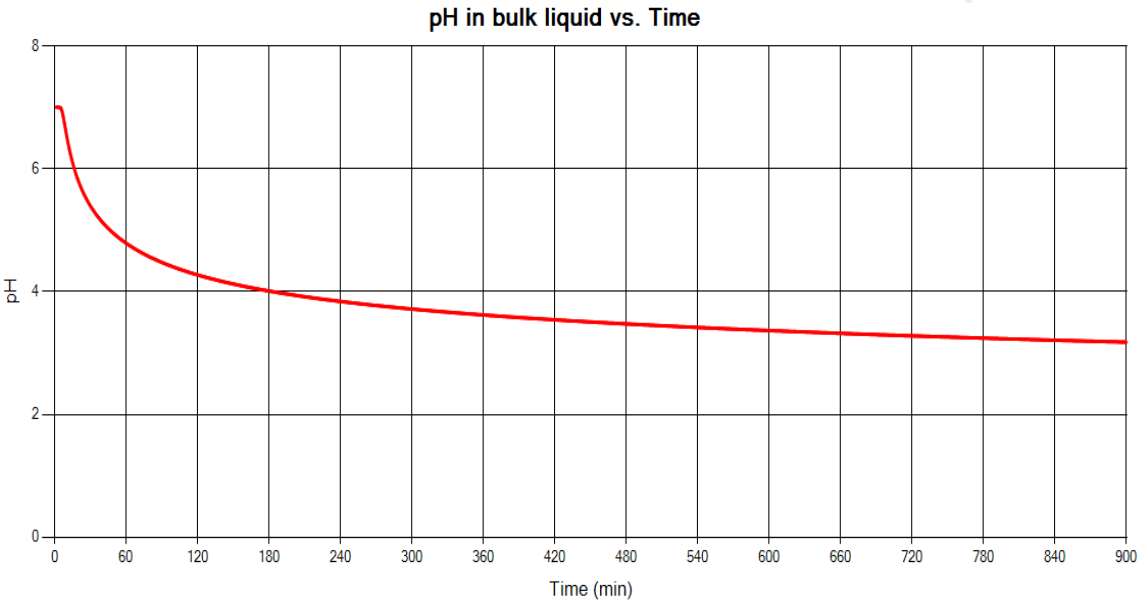

Figure 5. A plot of pH in bulk liquid over time.

Plots of glycerin concentration and local potential in the biofilm layer are shown in Figure 6 and 7. Thickness of the layer was set at 60 μm. The glycerin concentration increased in the early period due to diffusion of glycerin from the bulk liquid into the biofilm layer. The concentration, however, subsequently decreased since glycerin was consumed by the bacteria. The potentials quickly increased in the early period and at a slower rate afterwards. The potentials close to the anode were slightly higher than those close to the bulk liquid. As a result, the generated electrons flowed toward the anode with the higher potential, and the current flowed in the opposite direction.

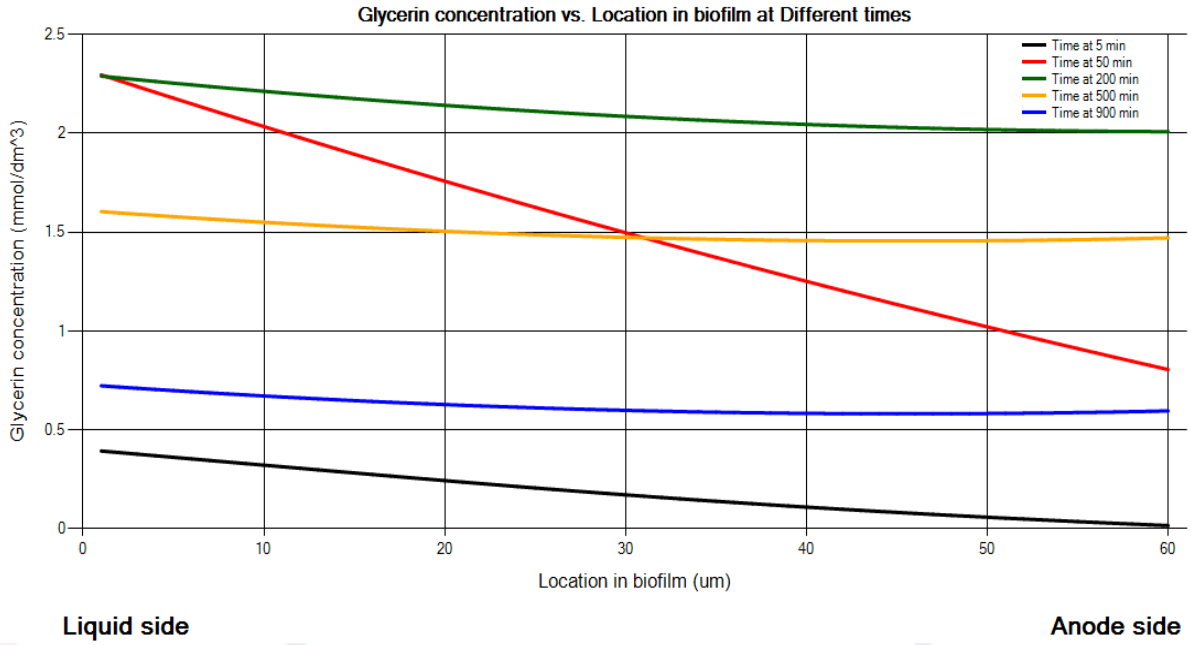

Figure 6. Plots of glycerin concentration in biofilm layer at different times.

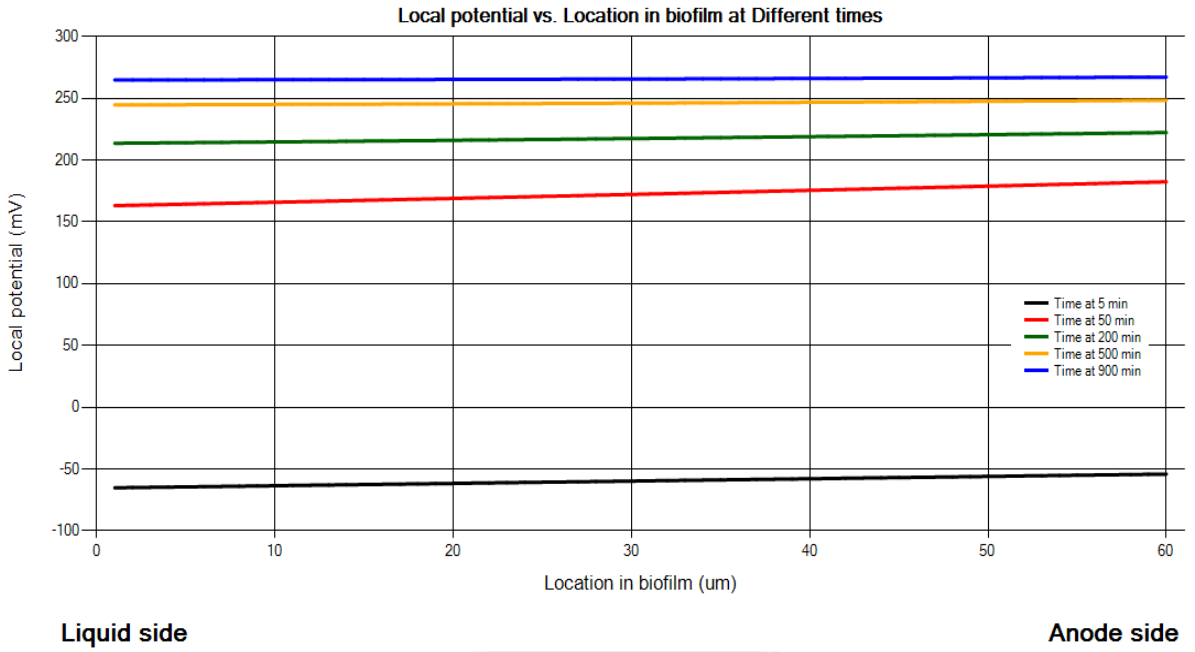

Figure 7. Plots of local potential in biofilm layer at different times.

Plots of cathode, anode, and MFC open-circuit voltages of the system are shown in Figure 8. The cathode voltage increased over time, since more hydrogen ions accumulated in the system and participated in the reduction reaction. The anode voltage also increased over time, since the glycerin concentration decreased, therefore the rate of electron generation decreased. Fewer number of electrons means the anode becomes more positive; thus a higher voltage. Compared to the anode voltage, the cathode voltage increased at a faster rate in the first half

of the operation time, but in the end both voltages became steady. As a result, the open-circuit voltage slightly increased in the first half, but became steady in the end.

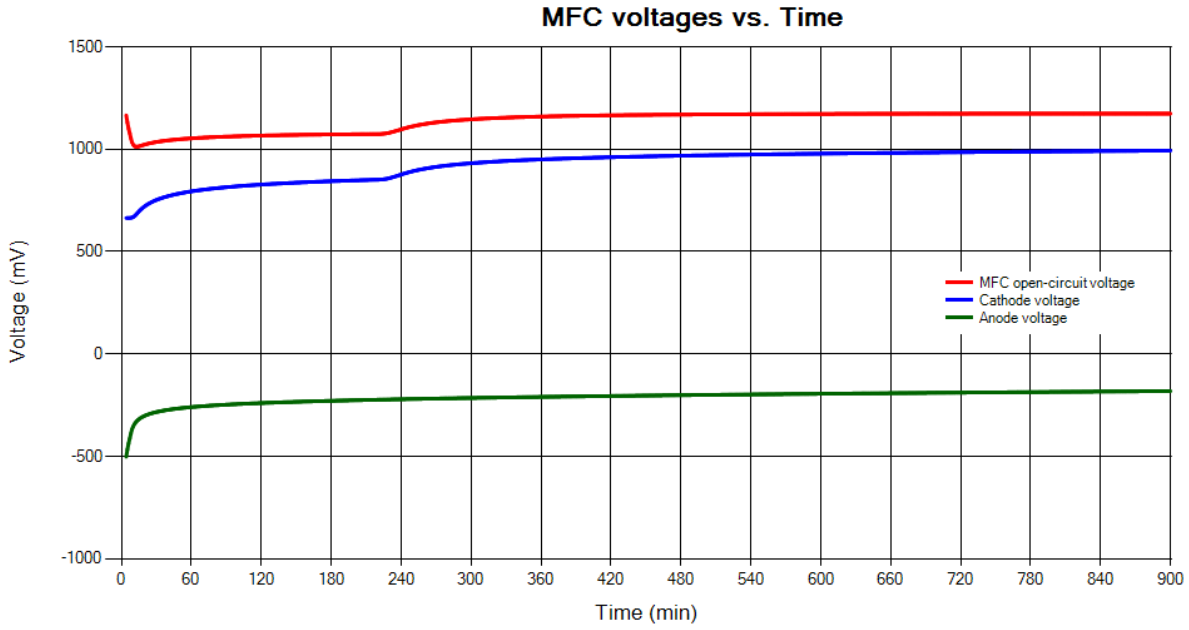

Figure 8. Plots of cathode, anode, and MFC open-circuit voltages over time.

The simulation program was able to compute and provide the voltages and the concentration profiles of chemical species in the MFC, and the trends seemed to agree with our expectations. Further development of the program involves calculation of the current and power density of the system. In addition, model validation with experimental data is necessary and more accurate model parameters are desirable, before the program could be used in practical optimization and prediction of the MFC performance.

References

Conte, S. D., and de Boor, C. (1980) The solution of linear system by elimination. *Elementary Numerical Analysis* (pp. 147-157): McGraw-Hill.

Feng, Y., Yang, Q., Wang, X., Liu, Y., Lee, H., and Ren, N. (2011) Treatment of biodiesel production wastes with simultaneous electricity generation using a single-chamber microbial fuel cell. *Bioresource Technology, 102*(1), 411-415.

Kato Marcus, A., Torres, C. I., and Rittmann, B. E. (2007) Conduction-based modeling of the biofilm anode of a microbial fuel cell. *Biotechnology and Bioengineering, 98*(6), 1171-1182.

Liu, H., and Logan, B. E. (2004) Electricity generation using an air-cathode single chamber microbial fuel cell in the presence and absence of a proton exchange membrane. *Environmental Science & Technology, 38*(14), 4040-4046.

Logan, B. E., Hamelers, B., Rozendal, R., Schröder, U., Keller, J., Freguia, S., Aelterman, P., Verstraete, W., and Rabaey, K. (2006) Microbial fuel cells: methodology and technology. *Environmental Science & Technology, 40*(17), 5181-5192.

Merkey, B. V., and Chopp, D. L. (2012) The performance of a microbial fuel cell depends strongly on anode geometry: a multidimensional modeling study. *Bulletin of Mathematical Biology, 74*(4), 834-857.

Selembo, P. A., Perez, J. M., Lloyd, W. A., and Logan, B. E. (2009) High hydrogen production from glycerol or glucose by electrohydrogenesis using microbial electrolysis cells. *International Journal of Hydrogen Energy, 34*(13), 5373-5381.

Stewart, P. S. (2003) Diffusion in biofilms. *Journal of Bacteriology, 185*(5), 1485-1491.

Thauer, R. K., Jungermann, K., and Decker, K. (1977) Energy conservation in chemotrophic anaerobic bacteria. *Bacteriological Reviews, 41*(1), 100-180.

Torres, C. I., Kato Marcus, A., and Rittmann, B. E. (2008) Proton transport inside the biofilm limits electrical current generation by anode-respiring bacteria. *Biotechnology and Bioengineering, 100*(5), 872-881.

Torres, C. I., Marcus, A. K., Lee, H.-S., Parameswaran, P., Krajmalnik-Brown, R., and Rittmann, B. E. (2010) A kinetic perspective on extracellular electron transfer by anode-respiring bacteria. *FEMS Microbiology Reviews, 34*(1), 3-17.

Zeng, Y., Choo, Y. F., Kim, B.-H., and Wu, P. (2010) Modelling and simulation of two-chamber microbial fuel cell. *Journal of Power Sources, 195*(1), 79-89.

Zhang, H., and Cloud, A. (2006, November 6 – 9). *The permeability characteristics of silicone rubber.* Paper presented at the Global Advances in Materials and Process Engineering, Dallas, Texas.

Zielke, E. A. (2006). Numerical analysis of a one dimensional diffusion equation for a single chamber microbial fuel cell using a linked simulation optimization (LSO) technique. *E521: Advanced Numerical Methods*.

iafor